

Processing issues related to the bi-dimensional ionic conductivity of BIMEVOX ceramics

Paul Fuierer · Russell Maier · Ulla Röder-Roith ·
Ralf Moos

Received: 24 February 2011 / Accepted: 17 March 2011 / Published online: 9 April 2011
© Springer Science+Business Media, LLC 2011

Abstract Bismuth vanadate, $\text{Bi}_4\text{V}_2\text{O}_{11}$, and its doped variations, $\text{Bi}_4(\text{Co}_{0.15}\text{V}_{0.85})_2\text{O}_{11}$, $\text{Bi}_4(\text{Cu}_{0.1}\text{V}_{0.9})_2\text{O}_{11}$, and $\text{Bi}_4(\text{Cu}_{0.05}\text{Ti}_{0.05}\text{V}_{0.90})_2\text{O}_{11}$ are investigated with respect to relative processability and total conductivity. In conventionally prepared (pressure-less sintered) ceramic disks, the single-substitution compounds show signs of exaggerated grain growth with significant *c*-axis preferred orientation. The doubly substituted $\text{Bi}_4(\text{Cu}_{0.05}\text{Ti}_{0.05}\text{V}_{0.90})_2\text{O}_{11}$ is found to have the widest processing window, resulting in sintered monoliths with the highest relative density and no preferred orientation. It also shows the highest conductivity ($7 \times 10^{-2} (\Omega\text{cm})^{-1}$) at 500 °C, as measured by impedance spectroscopy. Activation energies for conduction of the four compounds are reported and found to be comparable to earlier study. Hot forged samples of $\text{Bi}_4(\text{Cu}_{0.05}\text{Ti}_{0.05}\text{V}_{0.90})_2\text{O}_{11}$ are prepared for the first time, with only moderate texturing achieved. We assert that the lack of texture in $\text{Bi}_4(\text{Cu}_{0.05}\text{Ti}_{0.05}\text{V}_{0.90})_2\text{O}_{11}$ is responsible for the higher conductivity measured through the sample thickness when compared to $\text{Bi}_4(\text{Co}_{0.15}\text{V}_{0.85})_2\text{O}_{11}$, $\text{Bi}_4(\text{Cu}_{0.1}\text{V}_{0.9})_2\text{O}_{11}$ and other related compounds.

Introduction

Along with “green” technologies comes renewed interest in functional ceramics for solid oxide fuel cells, gas sensors, catalysts, and gas separation membranes. Bismuth vanadate or $\text{Bi}_4\text{V}_2\text{O}_{11}$ (abbreviated as BIVOX) and related compounds with different chemical substitutions, including $\text{Bi}_4(\text{Co}_x\text{V}_{1-x})_2\text{O}_{11}$ (BICOVOX) and $\text{Bi}_4(\text{Cu}_x\text{V}_{1-x})_2\text{O}_{11}$ (BICUVOX), have high oxygen conductivity and exchange characteristics that make them potential candidates for these applications [1–5]. As proposed by Abrahams and Krok [6], the mechanism for high oxygen ion conductivity depends on the polarizability of the bismuth ions, the variable coordination of the vanadium ions, and the large oxygen vacancy concentration. The oxygen conductivity of such compounds has been reported to be greater than that of state of the art stabilized zirconia, particularly at moderate temperatures of around 500 °C [6, 7].

BIMEVOX (ME: Cu^{2+} , Co^{2+} , Ni^{2+} , Ti^{4+} etc.) is an acronym representing this group of solid oxide electrolytes. The crystal structure can be generally described as an alternate stacking of $(\text{Bi}_2\text{O}_2)^{2+}$ layers and $[(\text{V}/\text{ME})\text{O}_{3.5}]^{2-}$ perovskite sheets. Several groups have reported analysis of the structure using powders or single crystals [8–11]. Details vary due to superstructure modulations and variations in defect concentrations, but the room temperature structure (α -phase) of BIVOX is usually found to be orthorhombic, with cell parameters around $a = 5.53 \text{ \AA}$, $b = 5.61 \text{ \AA}$, and $c = 15.3 \text{ \AA}$ for the basic mean cell, and $a = 16.6 \text{ \AA}$, $b = 5.61 \text{ \AA}$, and $c = 15.3 \text{ \AA}$ for the superstructure cell (with tripled cell volume) [9, 10]. The compound then undergoes a series of transitions with increasing temperature ($\alpha \rightarrow \beta \rightarrow \gamma$) with the high temperature phase having tetragonal symmetry and high ionic conductivity above about 570 °C. Structural refinement of the high

P. Fuierer (✉)
Department of Materials and Metallurgical Engineering,
New Mexico Institute of Mining and Technology, Socorro,
NM 87801, USA
e-mail: fuierer@nmt.edu

R. Maier
Materials Research Laboratory, The Pennsylvania State
University, University Park, PA 16802, USA

U. Röder-Roith · R. Moos
Functional Materials Laboratory, University of Bayreuth,
95447 Bayreuth, Germany

temperature X-ray data gives space group I4/mmm, with $a = 3.988 \text{ \AA}$ and $c = 15.42 \text{ \AA}$ for the γ -phase [9], with high concentration of disordered oxygen ion vacancies which serve to conduct oxygen ions. This γ -phase can be stabilized at room temperature by the aliovalent substitutions mentioned above. The amount of substitution for vanadium varies depending on specific ion, but is usually around 10–15 at.% [11]. BICOVOX and BICUVOX ($\text{Me} = \text{Cu}$ or Co) have received most attention in the literature. While BICUVOX can exhibit increases in electron transference number and phase instability issues with reduced oxygen partial pressure, doubly substituted compounds have shown some improvements [12]. Some of the highest conductivities have been reported for double substitution compound $\text{Bi}_2\text{V}_{0.9}\text{Cu}_{0.05}\text{Ti}_{0.05}\text{O}_{11}$ [13, 14].

Due to the layered structure, the conductivity of BIMEVOX compounds is expected to be anisotropic in nature, which has been demonstrated in BIVOX and BICOVOX [15–17]. For both single crystal and highly textured pellet samples (uniaxially pressed from the powder, textured by applying magnetic field), conductivity parallel to the $(\text{Bi}_2\text{O}_2)^{2+}$ layer (a – b plane) has been observed to be a few orders of magnitude higher than that perpendicular to the a – b plane [15]. Consequently, microstructural texturing may need to be considered for optimal performance of these materials. The grains in sintered BIMEVOX ceramics can grow to platelets as a consequence of the anisotropic crystal growth habit of the material. Methods such as sol–gel, modified sol–gel, co-precipitation, mechanical activation, and combustion synthesis have been reported to achieve small particle size materials which avoid this habit [18–21]. On the other hand, Roy and Fuierer [22] have recently used molten salt synthesis of γ -BICOVOX to enhance it. Generally, though, conventional solid-state reaction between oxides has been used to prepare BIMEVOX.

Simner et al. [23] pointed out a lack in synthesis information regarding these compounds, and thus carried out a detailed study of BICUVOX. Solid state sintering resulted in ceramics with densities above 95%, with grain size 6–8 μm , and conductivity at 400 °C of $2 \times 10^{-2} (\Omega\text{cm})^{-1}$. Steil et al. [24] studied the grain size dependence of electrical conductivity for BICOVOX. More recently, Steil et al. [25] conducted a sintering study of group V-substituted BIMEVOX ($\text{Me} = \text{Nb}, \text{Ta}, \text{Sb}$) using dilatometry, and found them to be more refractory and thermally stable than BICOVOX and BICUVOX. However, relatively little study has been done regarding processing-property relationships, especially for such complex oxides. Double substitution (for example Cu and Ti) has been done only recently, and texturing techniques have only been utilized on two occasions. Our objective is to determine the BIMEVOX ceramics with greatest potential for high bi-dimensional conductivity, and conduct texturing studies via hot-forging.

Experimental section

Along with BIVOX, three BIMEVOX compositions were chosen due to their high conductivities reported in the literature: $\text{Bi}_4(\text{Co}_{0.15}\text{V}_{0.85})_2\text{O}_{11}$ (BICOVOX), $\text{Bi}_4(\text{Cu}_{0.1}\text{V}_{0.9})_2\text{O}_{11}$ (BICUVOX), and $\text{Bi}_4(\text{Cu}_{0.05}\text{Ti}_{0.05}\text{V}_{0.90})_2\text{O}_{11}$ (BICUTIVOX). These were fabricated using established and consistent solid-state procedures. Stoichiometric amounts of reagent grade oxides (Bi_2O_3 , V_2O_5 , Co_3O_4 , CuO , and TiO_2) were combined and milled for 18 h in a planetary mill using zirconia media and cyclohexane liquid. After drying, each batch was calcined in air at 630 °C for 12 h and then re-milled for 16 h, and 2 wt% binder (polyethylene glycol, PEG 400) was added using acetone as solvent. Homogenized, screened powders were then pressed into $\frac{1}{2}$ inch diameter disks at a pressure of 200 MPa. Disks were sintered in air at temperatures ranging from 690 to 800 °C for a period of 10 h, followed by slow furnace cooling (~ 1 °C/min).

X-ray diffraction (Siemens D 500, $\text{CuK}\alpha$, 40 kV, 30 mA, calibrated using a Si standard) of all samples (powders and ceramic monoliths) was performed over a range of 2θ (20°–60°) to observe phase content, crystallinity, and signs of texture. Densities of sintered pellets were determined from mass and geometric measurements.

Impedance spectroscopy was performed on the densest samples using a two-electrode (through thickness) method. Surfaces of the disks were ground parallel and then polished using 9 μm diamond paste. Circular electrodes were deposited by first sputtering a 150 nm layer of gold, followed by application of gold paste to attach gold wire leads. A 30 min anneal step at 740 °C was used to completely cure the paste. A computer controlled test station integrating a small tube furnace and high resolution dielectric analyzer (Novocontrol Alpha-Analyser) was used to measure complex impedances over a range of frequencies from 0.1 to 10^6 Hz, while cooling from 700 to 200 °C in 25 °C intervals. Nyquist plots were constructed to separate bulk ceramic and electrode contributions to the total impedance. The total bulk resistance of the ceramic was obtained by fitting to the central semicircular arc and finding its intersection with the real (impedance) axis according to Cole–Cole analysis. Resistance values were then converted to material conductivity using electrode area and sample thickness dimensions. Arrhenius plots were used to calculate activation energies for conduction within different phase regimes.

Subsequently, BICUTIVOX specimens were prepared by hot-forging. The same procedures as above were used up through powder preparation, but taller cylindrical samples (~ 15 mm in height) were pressed and bisque-fired at 550 °C prior to forging. Hot-forging was performed by squeezing the specimen between two polished stabilized

zirconia ram surfaces inside a vertical clamshell furnace. Multiple combined heating/loading schedules were attempted to find appropriate forging conditions. A typical successful forge involved heating to 750 °C at 10 °C/min, increasing the load to maximum of 300 kg at 6 kg/min, holding at maximum load and temperature for 2 h, removal of load at 6 kg/min, followed by a 1 h hold at temperature, and finally furnace cooling at 2 °C/min. Densities of forged samples were determined by the Archimedes method.

Two surfaces of each sample were prepared for examination, the large surface perpendicular to the forging axis (FA) and a surface parallel to the FA (revealed by cross-sectioning). These surfaces were ground using 1200 grit SiC followed by a 0.5 µm colloidal alumina polish. They were then thermally etched at 700 °C for 10 min. The parallel and perpendicular surfaces of each sample were analyzed using X-ray diffraction, and the surfaces were examined using a field emission scanning electron microscope (Hitachi, S-800).

Results and discussion

Phase formation and sintering behavior

Figure 1 includes X-ray scans for calcined powder, remilled powder, and sintered monoliths of BICUTIVOX. Single phase material is retained throughout the process. Re-milled powders show significant broadening of peaks due to particle size reduction, but are still indexed to the same basic cell. Figure 2 shows diffraction scans from the major surface of each of the four compositions sintered at 800 °C. For BIVOX, indexing of peaks is according to the unit cell of the α -phase, with the orthorhombic splitting of peaks (020/200, 022/202, 024/204, 026/206, and the 133/313 couples) apparent. In the case of substituted BIMEVOX, indexing is according to the γ -phase tetragonal cell (space group I4/mmm). All prominent peaks are accounted for and the ceramics appear to be single phase with the exception of BICOVOX where, at this sintering temperature, three peaks appear indicated by (*). These are likely due to a bismuth-poor second phase BiVO₄ (PDF 14-0688) or Bi_{1.33}V₂O₆ (PDF 039-0105) [26, 27]. Significant *c*-axis texturing is observed in singly substituted compounds, especially BICUVOX as evidenced by increased (004), (006), and (008) reflections. As sintering temperature increases, exaggerated grain growth occurs with the formation of platelets whose large faces tend to be oriented along the surface. On the other hand, very little texturing is apparent in BICUTIVOX even at high sintering temperature.

Figure 3 shows density curves for pressure-less sintered compacts of the four compositions. In addition to suggesting optimum sintering temperatures, the graph illustrates the

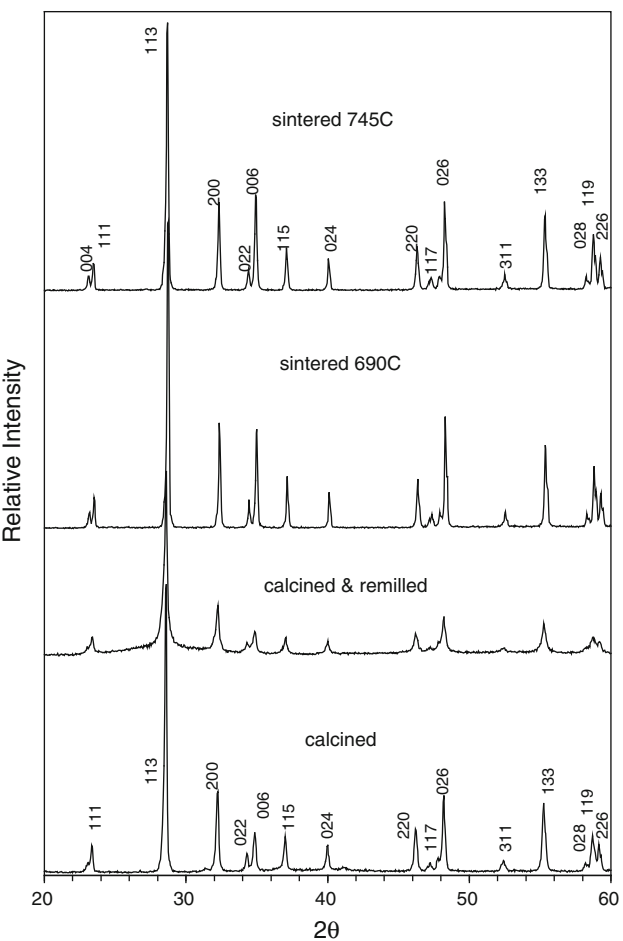


Fig. 1 X-ray diffraction scans of BICUTIVOX; powder after calcination at 630 °C, after remilling, and after sintering of monoliths. Indexing of peaks is according to the tetragonal unit cell of the γ -phase

relative ease with which the four compositions can be processed. BIVOX and BICUTIVOX display large windows for densification; minimal variation in density over the range investigated (690–800 °C). The sintering behavior was good, exhibiting high densities and normal grain growth. The single substitution compounds BICOVOX and BICUVOX on the other hand have limited process ranges, showing obvious signs of over-firing (exaggerated grain growth and loss of density) above about 750 °C. The average maximum density obtained for each composition are given in Table 1, and compared to theoretical values. Relative bulk densities (BD) are highest for the BIVOX and BICUTIVOX. The lower densities achieved in the single-substitution compounds may be attributed to porosity, vacancy defects, and/or formation of second phase(s). Micro-cracking may also be a culprit. As reported by Steil [24] for BICOVOX, the anisometric crystal growth above a critical size of platelet grains may induce excessive strain resulting in micro-cracks.

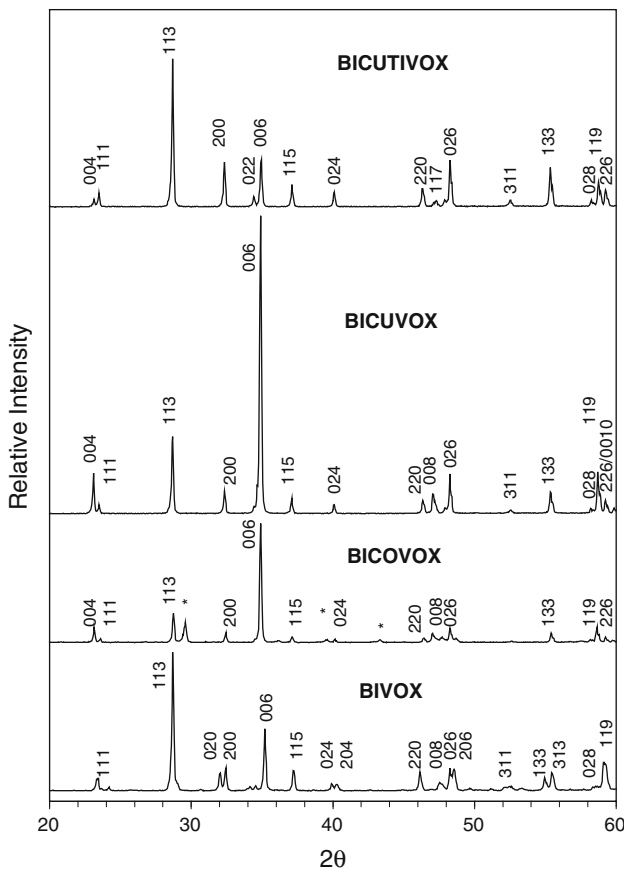


Fig. 2 X-ray diffraction scans of BIMEVOX pellets sintered at 800 °C. For BIVOX, indexing of peaks is according to the orthorhombic α -phase. For others, indexing is according to the tetragonal γ -phase

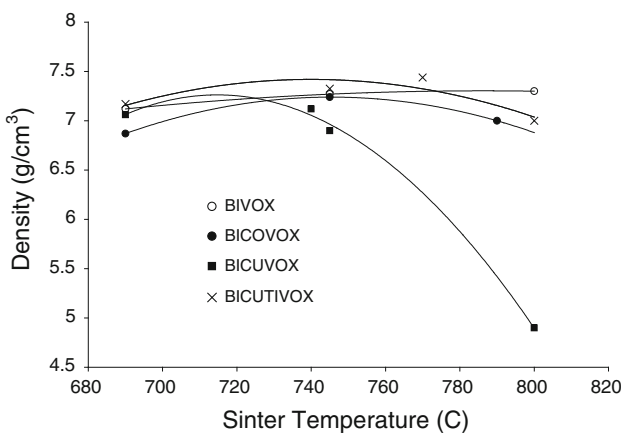


Fig. 3 Densification curves for BIVOX and BIMEVOX compositions

Conductivity

Figure 4 is a plot of total conductivity versus inverse temperature. Of the four compositions, BIVOX is seen to have the lowest conductivity at low temperatures, but the highest

conductivity at high temperature (>560 °C). BICUTIVOX has the highest conductivity at 500 °C, approaching 0.1 (Ωcm) $^{-1}$. Absolute total conductivity values at this temperature are in reasonable agreement with previous studies for all four compositions (see Table 2), and are presumed to be dominated by oxygen ion conduction.

The α - β - γ series of phase transitions is obvious in BIVOX as temperature is increased. The BIMEVOX compounds only exhibit a single change in slope, as expected, since the amount of dopant was chosen so as to stabilize the γ -phase at room temperature. This behavior is in agreement with reports for BICUTIVOX [13], BICUVOX [23, 28], and BICOVOX [11, 30]. The discontinuity is due to the γ' - γ phase transition, with an accompanying disordering of oxygen vacancies. The ordering at low temperature increases the activation energy for oxygen diffusion. The transition temperatures and activation energies from the current study are comparable to those found in the literature (Table 2), though different authors have reported different transition temperatures depending on exact composition and substitution level [28, 29]. For the BICOVOX sample, we found a significantly higher transition temperature (570 °C) than reported for stoichiometric BICOVOX. Lazure et al. [11] showed that this transition can be pushed to as high as 570 °C for excess Bi in solid solution (on vanadium sites). This is a plausible explanation for our sample, since at 800 °C, X-rays showed evidence of a Bi-poor 2nd phase, possibly leaving excess Bi in the BICOVOX phase. Fairly good agreement with literature is observed for the γ' (low temperature) activation energies, even though Krok et al. [30] pointed out that the conductivity of the γ' -phase depends on sintering conditions, density, etc.

Hot-forging and texture

Because of its superior sintering behavior and conductivity, BICUTIVOX was chosen for hot-forge studies. Sample height contraction during forging was on the order of 60%. Densities ranged from 7.33 to 7.55 g/cm³ (94–97% of theoretical). Figure 5 shows X-ray patterns from the large surface perpendicular to the FA and the cross-sectioned surface parallel to the FA. Comparison of the relative heights of the (006) and (200) peaks reveals some texturing. A semi-quantitative analysis can be done by calculating the Lotgering factor, f [31]:

$$f = \frac{p - p_0}{1 - p_0} \quad (1)$$

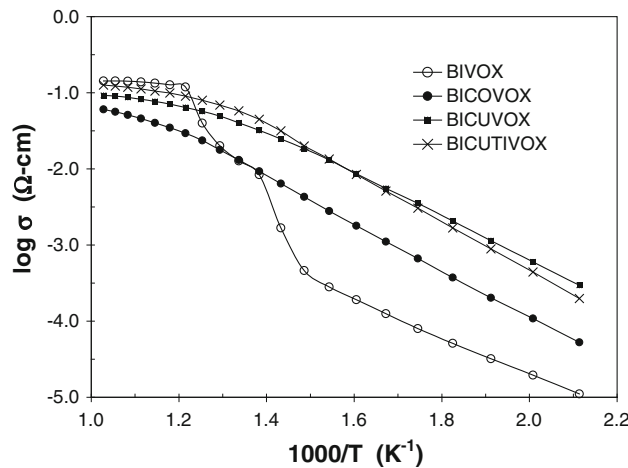
$$p = \frac{\sum_l I(00l)}{\sum_{hkl} I(hkl)} \quad (2)$$

where p is the ratio of the intensity of a peak of concern in a textured sample over the sum all reflections in the X-ray

Table 1 Bulk densities and *c*-axis orientation (Lotgering) factors, *f*, of sintered BIMEVOX and hot-forged BICUTIVOX. “*f*_s” is for the samples with maximum density and used for electrical measurements.

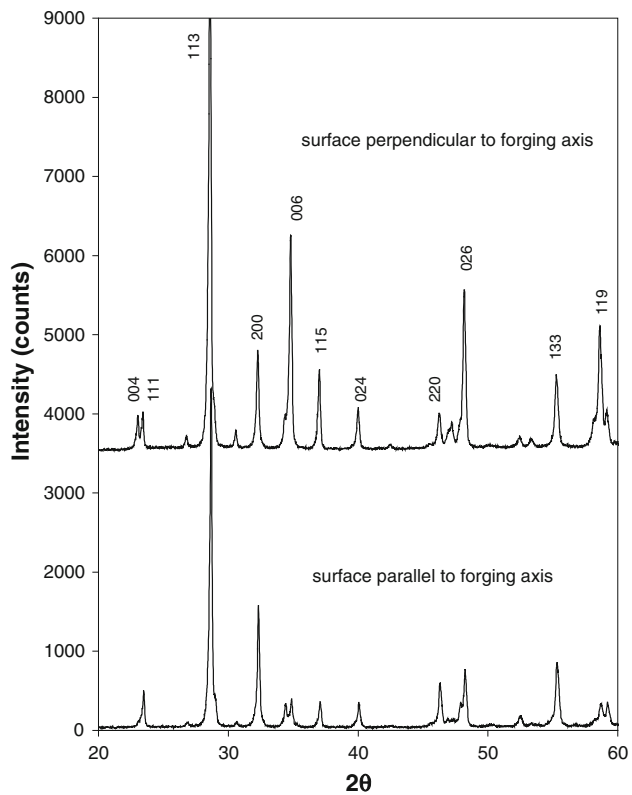
“*f*_{max}” represents maximum orientation observed for any sintering temperature. Theoretical (X-ray) densities are taken from Varma et al. [10]; Lazure et al. [11]; and Simner et al. [23]

	ρ , g/cm ³ (literature)	BD, g/cm ³ (sinter temp)	Relative density (%)	Lotgering <i>f</i> _s (%)	Lotgering <i>f</i> _{max} (%)
BIVOX	7.72	7.40 (800 °C)	96	12	15
BICOVOX.15	7.77	7.0 (790 °C)	91	57	57
BICUVOX.1	7.84	7.12 (740 °C)	91	8	54
BICUTIVOX.0505	7.81	7.44 (770 °C)	95	6	7
BICUTIVOX.0505 (Hot-forged)		7.55 (HF 750 °C)	97	11	11

**Fig. 4** Temperature dependence of the electrical conductivity for BIVOX and BIMEVOX. Partial substitution for vanadium by transition metals eliminates several intermediate phases seen in BIVOX, and stabilizes the conductivity into two temperature regimes, high and low**Table 2** Conductivity and phase transition parameters for BIMEVOX compared to previous literature (shown in parentheses)

	$\sigma @ 500 °C$, (Ωcm) ⁻¹ (literature)	$T(\gamma' - \gamma)$, °C (literature)	E_a (eV), γ' phase (literature)	E_a (eV), γ -phase (literature)
BIVOX	2.0×10^{-2}	$(\beta - \gamma)$ 550	(β) 0.91	(γ) 0.18
(Abraham et al. [9])	(1×10^{-2})	(525–550)	(0.94)	(0.17)
BICOVOX	1.8×10^{-2}	570	0.66	0.44
(Lazure et al. [11])	(1×10^{-2})	(515)	(0.66)	(0.49)
BICUVOX	4.9×10^{-2}	460	0.61	0.35
(Dygas et al. [28])	(3×10^{-2})	(470)	(0.67)	(0.43)
BICUTIVOX	6.9×10^{-2}	480	0.69	0.34
(Paydar et al. [13])	(8.6×10^{-2})	(495)	(0.74)	(0.42)

Activation energies are calculated from Arrhenius $\ln(\sigma T)$ plots

**Fig. 5** X-ray diffraction scans from two orthogonal surfaces of hot-forged BICUTIVOX. The sample shows moderate *c*-axis texture (Compare to Fig. 1)

plot, and p_o is the equivalent ratio for an un-textured (calcined powder) sample. This analysis reveals an orientation factor of only 11% in the forged sample. This is very low relative to other layered compounds forged by the author, whose Lotgering factors were found to be in excess of 90% [32–35]. It is even lower than the texture present in pressure-less sintered BICOVOX and BICUVOX, with both reaching over 50% *c*-axis orientation (Table 1).

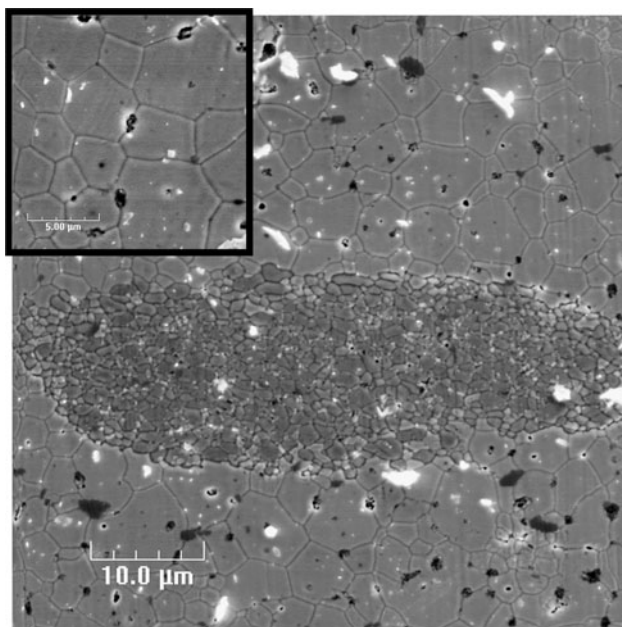


Fig. 6 Scanning electron micrographs of polished and thermally etched orthogonal surfaces of hot-forged BICUTIVOX. Disk-shaped domains of fine-grained material, whose short axes are parallel to the FA, are revealed in the cross-sectional surface. *Inset* is the plane perpendicular to the FA

Microstructure

Figure 6 shows micrographs of the hot-forged sample, both perpendicular and parallel surfaces. With hot-forging of Auriavillius and other layered structure ceramics, one expects a brick-wall type of grain organization in the parallel view. This is not the case here. Instead, we see a matrix of equiaxed grains of about 5 μm in size, with regularly spaced disk-shaped domains of very fine grained material on the order of 1 μm . These domains of fine-grained material have an elliptical cross-section, with a long axis of about 50 μm , and short axis of about 20 μm . They occur at an average spacing of about 100 μm . It appears that the contraction experienced during the forging process is a consequence of superplastic deformation via grain boundary sliding within the fine-grained regions of the compact. This is consistent with the observation that most of the contraction took place in the early stage of forging, followed by only minimal change in latter stages. This means there is very little or no pressure-enhanced, diffusional grain growth in the lateral direction which typically takes place in forging of other layered perovskites. We suspect that the titanium substitution in the material acts as a grain growth inhibitor via a solute drag mechanism, but details are yet unknown [36–38].

Conclusion

These results lead us to suspect that the high through-thickness conductivity of BICUTIVOX, measured in this study and reported by others, is due to a lack of the grain orientation effect that is observed in other BIMEVOX prepared by ordinary means. As has been demonstrated with BIVOX and BICOVOX, ionic conductivity is highest in the a - b crystallographic plane, which tends to naturally orient parallel to sample surfaces, effectively decreasing the through-thickness conductivity. BICUTIVOX samples do not show this orientation tendency, and therefore conductivity measurements tend to reveal random, polycrystalline isotropy and somewhat higher values. Even when hot-forged, this particular material will not form anisometric grains with preferred orientation. Instead, deformation takes place only via grain boundary sliding, and segregation of disk-shaped domains of fine grains develops as forging proceeds. In an attempt to maximize anisotropy and in-plane conductivity, we are now investigating forging behavior and directional grain growth of single-substitution BIMEVOX which show greater tendency for c -axis texture. Further investigation of grain-growth control in this family of functional ceramics is of interest.

Acknowledgements Funding from the Deutscher Akademischer Austauschdienst (DAAD) to support a summer research visit by the principal author to the University of Bayreuth is gratefully acknowledged.

References

- Pirovano C, Vannier RN, Capoen E, Nowogrocki G, Boivin JC, Mairesse G, Anne M, Dooryhee E, Strobel P (2003) Solid State Ionics 159:181
- Chetouani A, Taouk B B, Bordes-Richard E, Abi-Aad E, A-boukais A (2003) Appl Catal A 252:269
- Cho H, Sakai G, Shimano K, Yamazoe N (2005) Sensors Actuators B 109:307
- Kida T T, Minami T, Kishi S, Yasa M, Shimano K, Yamazoe N (2009) Sensors Actuators B 137:147
- Wang J, Ji B, Zhu X, Cong Y, Yang W (2009) Chin J Catal 30:926
- Abrahams I, Krok F (2003) Solid State Ionics 157:139
- Abraham F, Boivin J, Mairesse G, Nowogrocki G (1990) Solid State Ionics 40–41:934
- Muller C, Anne M, Bacmann M, Bonnet M (1998) J Solid State Chem 141:241
- Abraham F, Debremille-Gresse M, Mairesse G, Nowogrocki G (1988) Solid State Ionics 28–30:529
- Varma K, Subbanna G, Row T, Rao C (1990) J Mater Res 5:2718
- Lazure S, Vannier R, Nowogrocki G, Mairesse G, Muller C, Anne M, Strobel P (1995) J Mater Chem 5:1395
- Yaremchenko A, Kharton V, Naumovich E, Marques F (2002) Mater Chem Phys 77:552
- Paydar M, Hadian A, Fafilek G (2004) J Mater Sci 39:1357. doi: 10.1023/B:JMSC.0000013896.02030.9d

14. Emel'yanova Y, Tsygankova E, Petrova S, Buyanova E, Zhukovskii V (2007) Russ J Electrochem 43:737
15. Muller C, Chateigner D, Anne M, Bacmann M, Fouletier J, Rango P (1996) J Phys D 29:3106
16. Kim S, Miyayama M (1997) Solid State Ionics 104:295
17. Shantha K, Varma K (1997) Mater Res Bull 32:1581
18. Pell J, Ying J, Zur Loye H (1995) Mater Lett 25:157
19. Hervoches C, Steil M, Muccillo R (2004) Solid State Sci 6:173
20. Castro A, Millan P, Ricote J, Pardo L (2000) J Mater Chem 10:767
21. Roy B, Fuierer P (2009) J Mater Res 24:3078
22. Roy B, Fuierer P (2009) J Am Ceram Soc 92:520
23. Simmer S, Suarez-Sandoval D, Mackenzie J, Dunn B (1997) J Am Ceram Soc 80:2563
24. Steil M, Fouletier J, Kleitz M, Labrune P (1999) J Eur Ceram Soc 19:815
25. Steil M, Ratajczak F, Capoen E, Pirovano C, Vannier R, Mairesse G (2005) Solid State Ionics 176:2305
26. Powder Diffraction File card # 14-0688
27. Powder Diffraction File # 039-0105
28. Dygas J, Krok F, Bogusz W, Kurek P, Reiselhuber K, Breitner M (1994) Solid State Ionics 70–71:239
29. Keziosis A, Bogusz W, Krok F, Dygas J, Orliukas A, Abrahams I, Gebicki W (1999) Solid State Ionics 119:145
30. Krok F, Bogusz W, Kurek P, Jakubowski W, Dygas J, Bangobango D (1994) Solid State Ionics 70–71:211
31. Lotgering F (1959) J Inorg Nucl Chem 9:113
32. Fuierer P, Newnham R (1991) J. Amer. Ceram. Soc. 74:2876
33. Fuierer P, Shrout T, Newnham R (1992) In: Smart materials fabrication and materials for micro-electro-mechanical systems, MRS Symposium Proceedings, vol 276, Pittsburgh, p 51
34. Nichtawitz T, Fuierer P (1994) In: Pandey R, Liu M, Safari A (eds) Proceedings of 9th international symposium on applications of ferroelectrics. Pennsylvania USA, p 126
35. Shen Y, Clarke D, Fuierer P (2008) Appl Phys Lett 93:102907
36. Cahn J (1962) Acta Metall 10:789
37. Rahaman M, Zhou Y (1995) J Eur Ceram Soc 15:939
38. Rahaman M (2007) In: Ceramic processing. CRC Press, Boca Raton, p 398